# Modeling the Photophysics and Photochromic Potential of 1,2-Dihydronaphthalene (DHN): A Combined CASPT2//CASSCF-Topological and MMVB-Dynamical Investigation

**Gaia Tomasello,[†] Francois Ogliaro,[‡] Michael J. Bearpark,*[,§] Michael A. Robb,[§] and Marco Garavelli*[,†]**

*Dipartimento di Chimica "G. Ciamician", Università di Bologna, Via Selmi 2, I-40126 Bologna, Italy, Equipe de Chimie et Biochimie Théoriques, UMR 7565 - CNRS, Université Henri Poincaré, Nancy 1, BP 239, 54506 Vandoeuvre-lès-Nancy Cedex, France, and Department of Chemistry, Imperial College London, London SW7 2AZ U.K.*

*Received: March 26, 2008; Revised Manuscript Received: July 16, 2008*

The photochemical ring opening of 1,2-dihydronaphthalene (DHN) was investigated using two complementary computational approaches. CASPT2//CASSCF minimum energy paths were characterized for reaction channels on the three lowest-energy singlet excited states, describing initial evolution of the spectroscopic bright (ionic) state and its subsequent decay to dark (covalent) states of benzene-like and hexatriene-like character. Although the benzene-like state is unreactive and can radiate, the hexatriene-like state has indirect access to a low-energy conical intersection seam, at which radiationless decay to the ground state and subsequent product formation can take place. An MMVB molecular dynamics simulation was carried out on the reactive hexatriene-like excited state, suggesting that intramolecular vibrational energy redistribution (IVR) controls the radiationless decay and the photoproduct distribution (which is qualitatively reproduced).

## 1. Introduction

Photochromism[1,2] is the reversible transformation of a single chemical species between two isomers having different absorption spectra, with the transition in at least one direction being induced by light.[3] Several classes of organic compounds show this behavior, but currently the most important group of photochromic systems is based on pericyclic reactions.[4,5] These photochromic systems have been studied because of their potential technological applications in the form of optical devices, molecular switches, or for data storage.[6] Examples include fulgides[7,8] and diarylethenes,[9] which are "two-way" photochromic systems because their open and closed forms are interconverted in both directions when irradiated at suitable different wavelengths. On the other hand, the dihydroazulene/vinylheptafulvene[10,11] couple is an example of "one-way" photochromism, because the back-reaction occurs only thermally (unless a higher state is excited[12]).

Of the many pericyclic reactions, electrocyclizations have proved to be especially suitable as a basis for photochromism. The $4n + 2$ systems whose photochromism results from an electrocyclic 1,3,5-hexatriene/1,3-cyclohexadiene interconversion[13] comprise a very large number of species. In particular, ten-electron photochromism ($n = 2$) has been shown to be a possible concept for molecular switching, and 1,1-dicyano-dihydroazulene (DHA)[10,14,15] is the most versatile compound of this class at present.

1,2-Dihydronaphthalene (DHN)[16] has also been studied as another potential example of ten-electron photochromism, and its photochemistry has been investigated for over 30 years.[17] Irradiation of DHN derivatives produces a complex mixture of many photoproducts, whose nature and amounts strongly depends on factors such as wavelength, substituents, temperature and others.[18] However, the principal photoproducts observed—those that seem to be independent of substituents—were *o*-quinodimethane ($Q_s$ in Figure 1, a product of the ring-opening reaction) and benzobicyclohexene (BBH in Figure 1, a further cyclization photoproduct).[19] This process was intensively studied during the seventies[20] because of its potential industrial application in vitamin D synthesis.

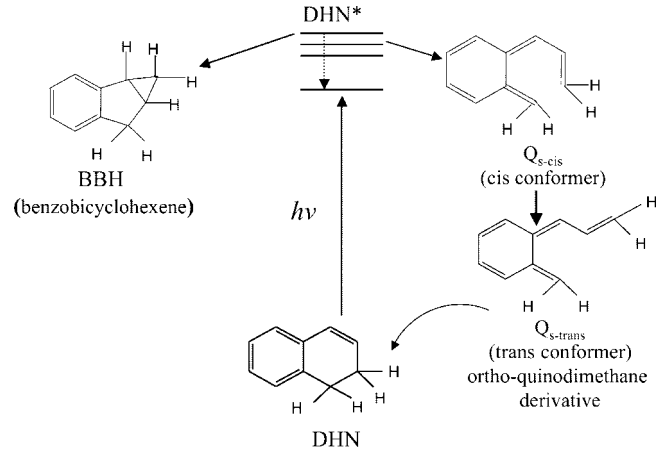


**Figure 1.** Photoproducts observed[16] after 1,2-dihydronaphthalene (DHN) is irradiated at around 250 nm.

The experimental evidence collected for DHN can be summarized as follows:

(i) A "two-photon" mechanism, two different photons in succession, was proposed by Salisbury[19] for BBH formation (Figure 2), based on finding that this photoproduct was observed only when two different light beams (one at 280 nm and the other at 400 nm) were both turned on. In this case, DHN first absorbs at the shorter wavelength, inducing a photochemically

* Corresponding author. E-mail: M.G., marco.garavelli@unibo.it; M.J.B., m.bearpark@imperial.ac.uk.
[†] Università di Bologna.
[‡] Université Henri Poincaré.
[§] Imperial College London.

10.1021/jp802613m CCC: $40.75 © 2008 American Chemical Society
Published on Web 09/12/2008

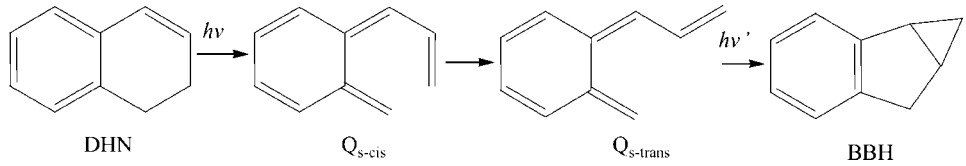


**Figure 2.** Proposed "two-photon"[19] mechanism for BBH formation from DHN.

allowed 6-electron conrotatory ring-opening reaction which leads to an s-cis o-quinodimethane intermediate ($Q_{s\text{-}cis}$), followed by thermal single-bond isomerization to the more stable s-trans conformer ($Q_{s\text{-}trans}$). A second photon at longer wavelength is then absorbed to give BBH through a 4 + 2 closure.[21]

(ii) However, disagreement appears in the literature about the two-photon mechanism and the problem of "short" and "long" wavelengths used for the photochemical reaction. Laarhoven et al.,[22] by studying 3-methyl-1,2-dihydronaphthalene photochemistry, supported the idea of the two-photon mechanism because production of BBH was observed by irradiating with broadband light. Nevertheless, the photochemistry of 3-methyl- and 4-methyl-1,2-dihydronaphthalene was also studied by Duguid and Morrison,[18] who reported ultraviolet absorption and fluorescence spectra both in the gas phase and in solution. In particular, they were interested in the photoproduct distribution from using narrow band light centered at 254 nm. This revealed that, despite the proposed two-photon mechanism, even a single photon at 254 nm is able to trigger the photochemical formation of BBH as well as other products.

(iii) Duguid and Morrison[23] also found that solvent polarity and acidity do not affect the quantum yield for BBH formation. This suggests that, if an ionic excited state is initially populated, it must be very quickly abandoned before any relevant part of the reaction coordinate toward BBH is accessed. Unfortunately, the nature of the spectroscopic state is not yet known experimentally.

(iv) Recently, the photoreactions of 1,1-dicyano-2,2-diphenyl-1,2-dihydronaphthalene (a potential photochrome of 1,2-dihydronaphthalene where HCN elimination is precluded by the presence of two phenyl groups) have been studied via time-resolved photochemical techniques by Daub and collaborators.[16] Also in this case, by using a single light beam of 250 nm, several photochemical processes were observed, including formation of both BBH and s-cis/s-trans $Q_s$. Notably, all three suggested photoprocesses (Figure 1) occurred on a time scale of less than 10 ns.

(v) Only weak fluorescence below 400 nm was observed for 1,1-dicyano-2,2-diphenyl-1,2-dihydronaphthalene in methylcyclohexane or ethanol, and there was virtually no phosphorescence in glassy media.[16] Additionally, Duguid and Morrison[18] reported the low fluorescence quantum yield (QY $\sim$ 0.003) of 3- and 4-methyl-1,2-dihydronaphthalene: analysis of the corrected fluorescence spectra in the gas phase revealed a main peak around 300 nm and a weaker peak around 400 nm.

The first goal of this computational study is to understand whether a one-photon mechanism is sufficient to explain the photophysics and photochemistry of the prototype DHN (and its derivatives such as 3- and 4-methyl-1,2-dihydronaphthalene, 1,1-dicyano-2,2-diphenyl-1,2-dihydronaphthalene) or whether it is necessary to invoke a two-photon mechanism for BBH formation.

As a second goal, this study is also part of an ongoing effort to understand photochromism[9,11,24−26] at a molecular level. Here for DHN, we decided to treat the initially populated ionic state explicitly, because the molecular motion responsible for the $\sigma$-bond cleavage begins on this state. We also used a wide range of computational methods (CASSCF, CASPT2, TDDFT, RASSI, MMVB dynamics) so that as many observables as possible, including molecular structure, geometry changes on excitation, absorption/emission spectra, and quantum yields can be calculated and compared with the experiments. After describing these methods and our results in detail, both static and dynamic information is combined into a single mechanistic scenario that explains the radiative and nonradiative processes involved in the singlet photochemistry and photophysics of DHN. A single-photon mechanism proves compatible with the experimental knowledge on DHN and its derivatives listed above, and the shape of the surface crossing mainly responsible for excited-state deactivation suggests that its photochromic potential is limited.

Finally, it is worth mentioning that we have not considered triplet states in this work. Experimentally, an attempt to generate DHN triplet states via sensitized excitation failed, and the ring-opening we have studied was assigned to a singlet state process on the basis (ref 16, p 4014) that "intersystem crossing does not occur at all". Reference 23 also argues that experimentally, "direct photolyses proceed via singlet chemistry". Furthermore, there is no obvious source of strong spin−orbit coupling in this system that would favor production of triplet states, on a time scale that would compete with any accessible singlet−singlet decay channel.

## 2. Computational Methods

**2.1. CASPT2//CASSCF Topology.** In this work, a CASPT2//CASSCF/6-31G* approach was used for reaction path calculations. First, CASSCF geometry optimizations and fully unconstrained minimum energy path (MEP)[27] computations were carried out using Gaussian 03.[28] The active space chosen was 10 electron in 10 orbitals: 10 $\pi,\pi^*$ orbitals for the open-ring isomer, and 8 $\pi,\pi^*$ plus 2 $\sigma,\sigma^*$ orbitals (describing the $\sigma$ bond which is broken) for the closed-ring DHN isomer. State averaging was used whenever two states became degenerate. Numerical frequency calculations were used to determine the nature of some of the optimized stationary points.

To account for dynamic electron correlation effects, which are more important for ionic excited states, and not well described by CASSCF using the above active space, CASPT2 energies were calculated using MOLCAS 5.0[29] at the geometries obtained with CASSCF. The energies referred to throughout the rest of this paper are CASPT2 energies at CASSCF geometries (CASPT2//CASSCF), unless stated otherwise. A note of caution: because we recover more dynamic electron correlation energy for an ionic excited state, we find that the ordering of the excited states is often changed with CASPT2 with respect to CASSCF. Furthermore, states that are degenerate with CASSCF at optimized crossing geometries may not give degenerate CASPT2 energies. Other geometries at which CASPT2 states are degenerate have not been reoptimized at this level and so represent upper bounds to the "true" crossing energies.

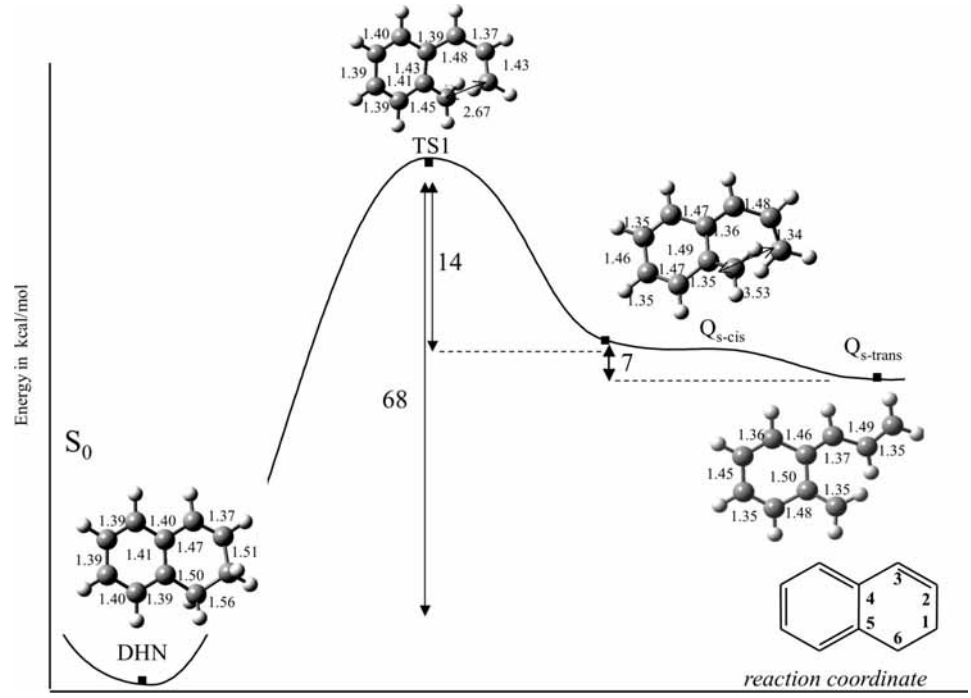


**Figure 3.** Ring-opening and isomerization pathways on the DHN ground state: CASPT2 energy values are reported in kcal/mol, and the bond lengths are in Å. The atom numbering used throughout this work is shown.

Transition dipole moments (TM) were estimated using the RASSI[30] method, also implemented in MOLCAS 5.0. These values, combined with CASPT2-corrected energies, were used to compute the oscillator strengths (*f*) according to the relation $f = (2/3)\mathrm{TM}^2/\Delta E$. Time-dependent density functional theory (TDDFT) (using the B3LYP functional[31−34] and 6-31G* basis set) was also used for this purpose. Although TDDFT calculations can reproduce the vertical excitation energies for states that are predominately single excitations, in general they overestimate the energies of doubly excited states such as the covalent low-energy dark state[35,36] here.

**2.2. MMVB Dynamics.** The relaxation channels defined by CASPT2//CASSCF describe the evolution of a vibrationally "cold" photoexcited molecule (i.e., one having infinitesimal kinetic energy). This approximation can fail: molecular dynamics often plays a key role in photochemical processes. In studying DHN, we found that the changes in geometry following initial relaxation on the excited states are *not* those that lead directly to crossings with the ground state. Consequently, modeling intramolecular vibrational-energy redistribution (IVR) is essential to know whether these crossings are accessible indirectly (and hence whether radiationless decay will be efficient) or not. Similar behavior has already been found for the photochromic diarylethylenes[9] and other systems.[37,38]

The CASSCF method is presently too expensive to carry out multiple trajectory calculations for a molecule the size of DHN. Instead, we used the hybrid molecular mechanics valence bond (MMVB)[39−43] method for nonadiabatic molecular dynamics simulations[44,45] from the reactive covalent $S_1$ state. MMVB is a parametrized method that emulates CASSCF,[46] but which is many orders of magnitude faster, using an "active space" (defining parametrized VB interactions) equivalent to CASSCF throughout. MMVB is therefore able to describe the $\sigma$-bond breaking and subsequent reorganization of the $\pi$-system of DHN. MMVB and CASSCF geometries for the relevant excited- and ground-state stationary points are in good agreement (MMVB was in fact used to generate the starting geometries for CASSCF optimizations). But the MMVB energies are not as good; in particular, the relative energies of open- and closed-ring structures are not well reproduced.[40,42] Because of this, and because it cannot describe[43] the spectroscopic state excited initially, MMVB dynamics does not offer a way to realistically predict the excited-state lifetime of DHN, as only the covalent excited $S_1$ surfaces can be explored, although this can still give an indication of product quantum yields.[47]

Direct on-the-fly dynamics was used (using the "trust region" method),[48,49] which does not require the potential energy surface to be fully computed in advance. Surface hopping[44] was used to evaluate the strong nonadiabatic coupling in the state-crossing region where population transfer occurs. The nuclear wavepacket distribution was emulated by running a "swarm" of many such semiclassical trajectories. To investigate whether trajectories can access the crossings, the starting geometries were the nearest excited-state bottlenecks. For the closed-ring isomer, this was an $S_1$ transition state[9] (TS*1): the sampling to generate the initial conditions was done on $S_1$, and the transition vector populated by a small (2 kcal/mol or so) amount of energy, with the remaining zero-point energy distributed among the remaining 3N-7 vibrational normal modes. (This transition structure TS*1 was selected as it is a well-defined bottleneck leading to the crossing region. As we discuss in section 3.2 below, it may not be the lowest-energy pathway, but it is the pathway that can be optimized with MMVB). In contrast, for the open-ring isomer we used the FC geometry, and the sampling required to define the initial geometries and velocities was carried out on the ground state. A total of 102 trajectories were computed: 52 starting from TS*1 on the closed-ring side and 50 starting from the FC geometry on the open-ring side. All trajectories were run for 1−3 ps, using a development version of Gaussian.

## 3. Results and Discussion

This section is split into four parts. In subsection 3.1 we discuss the structures and reaction paths computed on the ground state, $S_0$, whereas in subsection 3.2 we describe the different reaction paths and minimum energy structures initially optimized

**TABLE 1: TDDFT B3LYP/6-31G* and CASPT2/6-31G* Relative Energies ($\Delta E$) for Vertical Singlet Excitation Energies and Oscillator Strengths ($f$)[a]**

| | | TDDFT ($\Delta E$) | | | | CASPT2 ($\Delta E$) | | | |
|---|---|---|---|---|---|---|---|---|---|
| structures | states | kcal/mol | nm | $f$ | $\Psi$ | kcal/mol | nm | $f$ | $\Psi$ |
| DHN | $S_0$ | 0.0 | | | | 0.0 | | | |
| | $S_1$ | 109.05 | 262 | 0.176 | $\pi_{ex} \rightarrow \pi^*_{ex}$ | 101.97 | 283 | $8.79 \cdot 10^{-5}$ | $\pi_{bz1} \rightarrow \pi^*_{ex}$ $\pi_{ex} \rightarrow \pi^*_{bz1}$ |
| | $S_2$ | 111.04 | 257 | 0.018 | $\pi_{bz1} \rightarrow \pi^*_{ex}$ $\pi_{ex} \rightarrow \pi^*_{bz1}$ | 112.72 | 253 | 0.32 | $\pi_{ex} \rightarrow \pi^*_{ex}$ |
| | $S_3$ | 133.99 | 213 | 0.277 | $\pi_{bz2} \rightarrow \pi^*_{ex}$ $\pi_{ex} \rightarrow \pi^*_{bz2}$ | 141.37 | 202 | $3.05 \cdot 10^{-4}$ | $(\pi_{ex} \rightarrow \pi^*_{ex})^2$ |
| $Q_{s\text{-}cis}$ | $S_0$ | 0.0 | | | | | | | |
| | $S_1$ | 61.69 | 463 | 0.129 | | | | | |
| | $S_2$ | 93.26 | 306 | 0.007 | | | | | |
| | $S_3$ | 106.98 | 267 | 0.079 | | | | | |
| $Q_{s\text{-}trans}$ | $S_0$ | 0.0 | | | | 0.0 | | | |
| | $S_1$ | 68.79 | 415 | 0.209 | | 81.91 | 348 | | |
| | $S_2$ | 95.69 | 298 | 0.006 | | 85.35 | 334 | | |
| | $S_3$ | 109.68 | 260 | 0.013 | | 101.07 | 282 | | |

[a] A qualitative description of the wavefunctions for the different excited states is also reported (see Figure 4 for a description of the molecular orbitals involved).

on the first two singlet excited states $S_2$ and $S_1$. Subsection 3.3 deals with reaction paths leading to the $S_1/S_0$ crossing seam, at which radiationless decay to the ground state and subsequent product formation can take place. Molecular dynamics is presented and analyzed in subsection 3.4. Relative energies of the located critical points are summarized in Tables 1 and 2. The corresponding absolute energies are given in Table S1, whereas Tables S2−S4 summarize results from the dynamics (see Supporting Information).

**3.1. Ground-State $S_0$ Surface.** Two minima were initially located on the ground state: the closed-ring 1,2-dihydronaphthalene, DHN, and the s-trans open-ring *o*-quinodimethane, $Q_{s\text{-}trans}$ (Figure 3). The closed-ring DHN minimum is the lowest-energy structure, in agreement with experiment.

The ring-opening reaction on $S_0$ is strongly disfavored, because it involves a high-energy (68.4 kcal/mol) transition state (TS1) connecting DHN and $Q_{s\text{-}cis}$ (Figure 3). Although $Q_{s\text{-}cis}$ is a real minimum, a very small energy barrier (about 1 kcal/mol) separates it from the more stable (by about 7 kcal/mol) $Q_{s\text{-}trans}$ conformer. $Q_{s\text{-}cis}$ is therefore a metastable intermediate.

Finally, a benzobicyclohexene minimum BBH (Figure 1) was also located on $S_0$, 11 kcal/mol higher in energy than DHN.

**3.2. Vertical Excitation and Initial Relaxation from the Spectroscopic State.** Absorption spectra of 3-methyl- and 4-methyl-1,2-dihydronaphthalene reveal two different peaks: the first around 220 nm, more intense and more resolved, and the second, a broad band between 240 and 280 nm centered at 260 nm.[18] (The 1,1-dicyano-2,2-diphenyl-1,2-dihydronaphthalene absorption spectrum is also characterized by a main peak around 250 nm).

TDDFT calculations on the model DHN system (Table 1) assign these bands to optically active states $S_1$ and $S_3$: the computed absorption wavelengths are 262 and 213 nm, in good agreement with experiment. However, CASPT2 and RASSI reveal only a single spectroscopic state $S_2$ at 254 nm, with an oscillator strength of 0.32. This has the same nature as $S_1$ from TDDFT computations, and matches the experimental absorption at about 260 nm. Thus, although TDDFT reproduces both peaks of the absorption spectrum, CASPT2 "sees" only the lower energy one (assigning it to $S_2$): this is due to the restricted number (five) of CASSCF roots included in the state averaging procedure, which do not include the second bright state (see its wave function characterization in Table 1). Anyway, although TDDFT well reproduces the excitation spectrum, the energy of the dark states is overestimated with this method,[35,36] so we use CASPT2 state labels from now on. The spectroscopic state is therefore $S_2$ and ionic, described by a single HOMO → LUMO excitation. Correlation energy from CASPT2 computations is necessary for a reliable description of this state, as its energy is highly overestimated at the CASSCF level, for which it is the third singlet excited state at 169.18 kcal/mol (see Table 2).

Excitation energies and oscillator strengths for the open forms ($Q_{s\text{-}cis}$ and $Q_{s\text{-}trans}$) were also calculated with TDDFT, and the results (Table 1) reproduce the observed absorption band for the more stable s-trans isomer at 400 nm.

Figure 5 shows that the computed CASPT2//CASSCF MEP from the FC structure on $S_2$ is barrierless, and involves primarily the cyclohexadiene moiety. This pathway leads to a minimum $DHN^*_{CHD}$ but on the $S_1$ state, located 12.8 kcal/mol below the FC structure. $S_1$ at this minimum correlates with the vertically excited $S_2$ state: they both have a singly excited $1B_2$-like ionic character. The ring-opening reaction begins on the spectroscopic state $S_2$ (the $C_1-C_6$ $\sigma$-bond is highly stretched, going from 1.56 to 1.74 Å after relaxation), but it is not fully completed there.

Along this path, the $S_2$ state crosses (Figure 5) a dark benzene-like excited state ($S_1$ at the FC geometry, with a double excitation involving benzene orbitals; see Table 1 and Figure 4). This crossing (where the $C_1-C_6$ bond is 1.63 Å) may allow a partial internal conversion of the photoexcited population to the benzenic $S_1$ state, leading to the population of a second minimum $DHN^*_{bzn}$. This minimum is quite different from the one located on the ionic state $DHN^*_{CHD}$, with a geometry characterized by a benzene ring expansion according to the excitation, which is localized on the aromatic ring (see Figure 6).

Population splitting occurring through the $S_2/S_1$ conical intersection could explain the low intensity fluorescence features observed in these systems: 3- and 4-methyl-1,2-dihydronaphthalene fluorescence spectra reveal two different peaks, the main one at around 300 nm and a second one (much lower in intensity) at around 400 nm.[18] Accordingly, emission from the benzenic minimum $DHN^*_{bzn}$ and the ionic state intermediate $DHN^*_{CHD}$ have been calculated to be at 317 nm (90.13 kcal/mol) and 391 nm (73.18 kcal/mol), respectively, using the CASPT2 vertical energy gap between $S_1$ and $S_0$ for each structure (see Table 2). (For $DHN^*_{CHD}$, the gap is reduced by over 50 kcal/mol with CASPT2 compared to CASSCF; a characteristic of ionic states).

We now discuss the topology of the s-cis open-ring side of the potential energy surface, where another minimum was located on $S_1$ ($Q^*_{s\text{-}cis}$), corresponding to the relaxed ring-opened

**TABLE 2: CASSCF, CASPT2 and MMVB Energies (kcal/mol, Relative to DHN $S_0$) for All of the Molecular Structures Discussed in the Paper[a]**

| geometry | states | MMVB | CASPT2 | CASSCF |
|---|---|---|---|---|
| DHN | $S_0$ | 0 | 0 | 0 |
| | $S_1$ | 95.27 | 101.97 | 109.29 |
| | $S_2$ | | 112.72 | 169.18 |
| | $S_3$ | | 141.37 | 152.90 |
| | $S_4$ | | 159.34 | 175.77 |
| TS1 | $S_0$ | 79.02 | 68.39 | 65.92 |
| BBH | $S_0$ | | 11.54 | 17.66 |
| $Q_{s\text{-}cis}$ | $S_0$ | 72.06 | 54.35 | 41.45 |
| | $S_1$ | 183.01 | 146.64 | 149.41 |
| $Q_{s\text{-}trans}$ | $S_0$ | | 48.14 | 40.10 |
| | $S_1$ | | 130.04 | 136.01 |
| | $S_2$ | | 133.49 | 171.98 |
| | $S_3$ | | 149.20 | 159.48 |
| | $S_4$ | | 150.07 | 167.73 |
| $DHN^*_{bnz}$ | $S_0$ | 4.90 | 5.03 | 6.27 |
| | $S_1$ | 92.57 | 95.16 | 103.51 |
| $DHN^*_{CHD}$ | $S_0$ | | 26.77 | 33.07 |
| | $S_1$ | | 99.95 | 153.40 |
| | $S_2$ | | 111.83 | 126.39 |
| | $S_3$ | | 128.29 | 140.76 |
| TS*1 | $S_0$ | 76.98 | 60.34 | 67.13 |
| | $S_1$ | 150.82 | 111.86 | 127.56 |
| $Q^*_{s\text{-}cis}$ | $S_0$ | 86.98 | 70.98 | 69.63 |
| | $S_1$ | 144.10 | 96.56 | 108.68 |
| TS*2 | $S_0$ | | 95.73 | 103.21 |
| | $S_1$ | | 99.54 | 116.48 |
| TS*3 | $S_0$ | | 107.51 | 117.72 |
| | $S_1$ | | 107.76 | 124.10 |
| $CI1(S_1/S_0)$ | $S_0$ | 137.84 | 103.74 | 114.93 |
| | $S_1$ | 137.91 | 103.84 | 114.95 |
| $CI2(S_1/S_0)$ | $S_0$ | 136.96 | 109.31 | 123.32 |
| | $S_1$ | 137.15 | 111.60 | 123.42 |
| $CI3(S_1/S_0)$ | $S_0$ | 116.09 | 117.38 | 137.83 |
| | $S_1$ | 116.12 | 117.93 | 138.47 |
| $CI4(S_1/S_0)$ | $S_0$ | 126.59 | 113.94 | 131.14 |
| | $S_1$ | 126.72 | 110.94 | 131.19 |
| $CI5(S_1/S_0)$ | $S_0$ | | 147.55 | 154.17 |
| | $S_1$ | | 145.29 | 154.19 |
| $CI(S_2/S_1)$ | $S_1$ | | 100.61 | |
| | $S_2$ | | 101.26 | |
| | $S_3$ | | 127.11 | |
| $CI(S_3/S_2/S_1)$ | $S_1$ | | 118.49 | |
| | $S_2$ | | 120.09 | |
| | $S_3$ | | 120.20 | |

[a] Electronic states ($S_0$−$S_4$) are labeled according to CASPT2 energy order and each line of the table defines the same electronic state (note that the CASPT2 and CASSCF states energy ordering is not always the same).

structure ($C_1$−$C_6$ = 2.54 Å) and characterized by a covalent ($2A_1$-like) doubly excited $(\pi_{ex} \rightarrow \pi^*_{ex})^2$ wave function involving the hexatriene moiety. This point is similar to the excited-state minimum previously found for the cZc-hexatriene/1,3-cyclohexadiene[50] interconversion. (Note that we do not investigate in detail the relaxation from the spectroscopic state of the s-cis open-ring reactant, because it is not thermodynamically stable; although we have used it as the starting point for dynamics calculations later).

A transition state on $S_1$ (TS*1) connects the two covalent minima ($DHN^*_{bzn}$ and $Q^*_{s\text{-}cis}$, Figure 6) and describes an adiabatic ring-opening process (i.e., $C_1$−$C_6$ bond breaking). The corresponding CASPT2//CASSCF activation barrier (16 kcal/mol) is too high to account for the observed photoinduced ring-opening, weak fluorescence (from efficient radiationless decay) and the recorded excited-state kinetics (photoproducts are collected on a ns time scale),[16] calling for another and more efficient ring-opening route.

To better explain the ring-opening reaction occurring on the excited state, we searched for a reaction pathway connecting the ionic minimum $DHN^*_{CHD}$ (which is directly populated by decay from the FC region and already has a highly stretched $C_1$−$C_6$ bond) and the open-ring covalent minimum ($Q^*_{s\text{-}cis}$). Figure 7 shows the energy profile along a linear interpolation between these two points. Along this path, a change in the wave function of the $S_1$ state is expected, from ionic ($1B_2$-like) as in $DHN^*_{CHD}$ to covalent ($2A_1$-like) as in $Q^*_{s\text{-}cis}$.

CASPT2 energy profiles show that, as the system moves along the ring-opening coordinate, a triple degeneracy point $CI(S_3/S_2/S_1)$ (where the $C_1$−$C_6$ bond length is 2.10 Å) is in fact encountered (Table 2), which explains the change in the nature of the $S_1$ wave function that occurs on going from $DHN^*_{CHD}$ to $Q^*_{s\text{-}cis}$. Due to the incorrect CASSCF description of both the topology and the energetic order of these three states, a reliable optimization cannot be performed for the barrier for the ring-opening process at this level: this triple degeneracy does not exist along the CASSCF energy profiles. Thus, the "correct" path should be computed at a fully correlated (i.e., PT2) level. Unfortunately, PT2 optimizations are too expensive at present and we have limited our investigation to linear interpolations as a rough estimate of the real reaction path. The calculated energy barrier to reach the crossing-point (about 18 kcal/mol above $DHN^*_{CHD}$) therefore represents an upper limit for the barrier along the real path.

The reason for favoring the Figure 7 pathway over the Figure 6 one, even though both are found to have comparable barrier heights here, is as follows. Figure 6 represents an adiabatic $S_1$ reaction path with two excited-state minima (closed- and open-ring) and an optimized TS connecting them with a corrected CASPT2 energy barrier that is still high. We justify the "ionic" reaction path starting from $S_2$ relaxation (Figures 5 and 7) because, although the adiabatic transition state (Figure 6) is already an optimized point on a covalent state, with little further chance to get a lower value of energy, the triple degeneracy point (also able to explain how the system reaches the open-ring side) is an upper limit, not yet possible to optimize with CASPT2, which is the only method correctly reproducing the state order. Consequently, for this pathway, we expect the real barrier height to be lower. Furthermore, a more efficient route probably exists that bypasses the $CI(S_3/S_2/S_1)$ conical intersection point, passing around the cone on $S_1$ and involving a lower-energy avoided crossing TS. This would agree with the experimental observations, which suggest a much smaller energy barrier to account for the very weak fluorescence observed, and for the nanosecond time scale recorded for photoproduct formation.

In conclusion, the results collected in this section suggest the following picture for the initial photoinduced dynamics of DHN: a barrierless relaxation path in the spectroscopic state $S_2$ (which becomes $S_1$ along this reaction coordinate) drives the system out of the FC region toward a crossing that leads to population splitting. Two different minima may then be populated on the $S_1$ potential energy surface: $DHN^*_{CHD}$ and $DHN^*_{bzn}$, with ionic and benzenic character, respectively. $DHN^*_{CHD}$ has a geometry that is already prepared for ring opening (the $C_1$−$C_6$ bond length being 1.74 Å). From this minimum, the system may decay via a radiative process, accounting for the fluorescence feature observed at around 400 nm, whereas the more intense fluorescence feature (observed at around 300 nm) may be assigned to the unreactive benzenic minimum $DHN^*_{bzn}$. However, the very

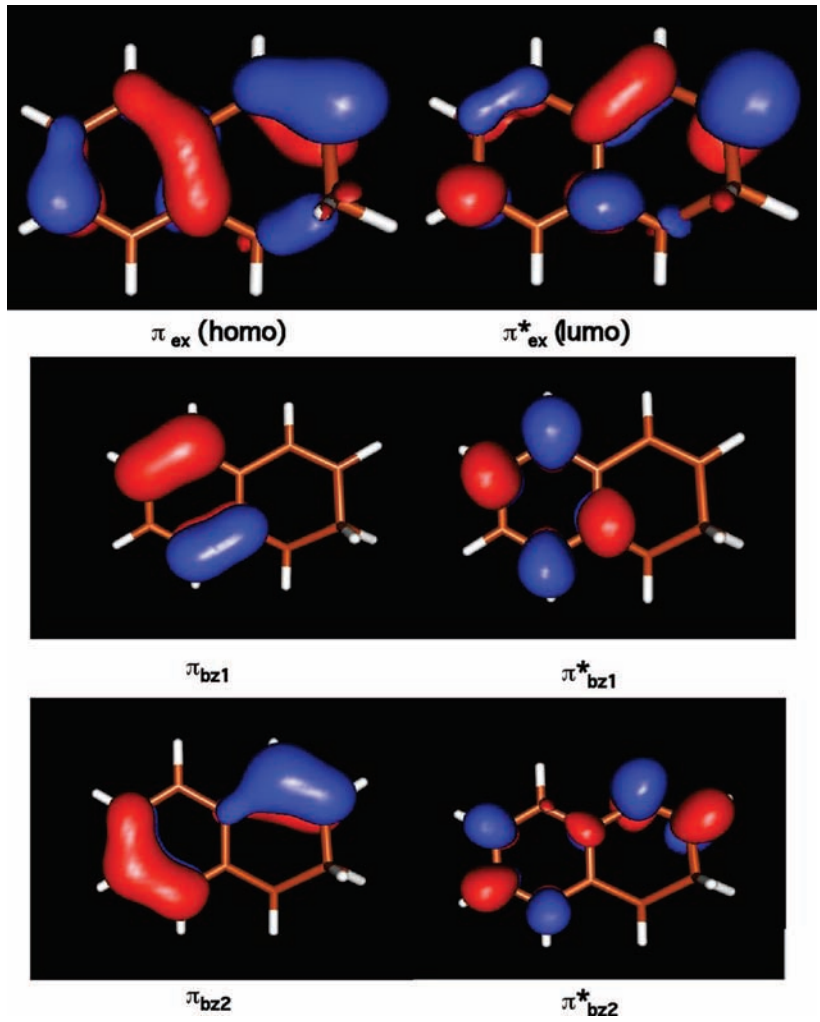


**Figure 4.** Orbitals involved in DHN low-energy singlet excited states.

weak fluorescence observed overall and the evidence that photoproducts are formed on a ns time scale suggests that motion away from these points must be favored. We think this finalizes the $C_1-C_6$ $\sigma$ bond breaking, involving a simultaneous reorganization of the $\pi$-electronic system leading the molecule to $Q^*_{s\text{-}cis}$ (an upper limit has been provided for the energy barrier along this channel). We anticipate here (and we will describe in more detail below) that a deactivation route exists that, moving along a different reaction coordinate, leads to a $S_1/S_0$ real crossing region where efficient internal conversion to the ground state may then occur.

**3.3. $S_1 \rightarrow S_0$ Radiationless Decay via Conical Intersections.** As anticipated above, a deactivation route exists from the $S_1$ minimum $Q^*_{s\text{-}cis}$ via an $S_1/S_0$ crossing region, where efficient internal conversion to the ground state may occur. This channel does not lie parallel to the initial reaction path, dominated by the $R_{1-6}$ increasing (i.e., $C_1-C_6$ $\sigma$ bond breaking). Instead, it involves a different coordinate, dominated by coordinate $R_{2-6}$ decreasing. A transition state TS*2 was located along this path at the CASSCF level, about 8 kcal/mol above $Q^*_{s\text{-}cis}$ (Figure 8), leading to an optimized conical intersection CI1. With CASPT2//CASSCF, the TS*2 structure is lower in energy than the conical intersection CI1, which is 7 kcal/mol above $Q^*_{s\text{-}cis}$, and at which the ground and excited states are still degenerate to within 1 kcal $mol^{-1}$.

We have also located a second related path (not shown), slightly higher in energy, along a different reaction coordinate $C_1-C_5$ (i.e., $R_{1-5}$), which connects $Q^*_{s\text{-}cis}$ to another $S_1/S_0$ conical intersection point, CI2. With CASSCF, there is a transition structure TS*3 linking $Q^*_{s\text{-}cis}$ and CI2; TS*3 is about 15 kcal $mol^{-1}$ above $Q^*_{s\text{-}cis}$ but less than 1 kcal $mol^{-1}$ above the crossing. As for TS*2 above, CASPT2 corrections appear to remove the transition state TS*3, which in this case becomes an $S_1/S_0$ crossing point itself at about 11 kcal/mol above $Q^*_{s\text{-}cis}$, i.e., only 4 kcal/mol higher than CI1.

In conclusion, these computations show that a low-lying, easily accessible, crossing region (CI1 and CI2) exists on the excited-state potential energy surface of DHN. These crossings are energetically accessible from $Q^*_{s\text{-}cis}$, but along different coordinates from the initial $\sigma$-bond that is broken; access to these crossings will therefore be controlled by molecular vibrations away from this reaction path.[9,37,38] Recently, we reported the existence of two conical intersections in the phenylbutadiene[25] systems that bear strong resemblance to CI1 and CI2.

The analysis of the molecular and electronic structure of these conical intersections allows a qualitative rationale for the observed DHN photoreactivity and photoproduct formation. Both crossings (CI1 and CI2) have a covalent nature, with the structural/electronic features typically found in covalent/covalent $S_1/S_0$ conical intersections of conjugated hydrocarbons and aromatic systems.[51] Indeed, both structures exhibit a tetraradicaloid nature, with a typical triangular arrangement (i.e., a kink) comprising three substantially unpaired $\pi$-electron centers (plus

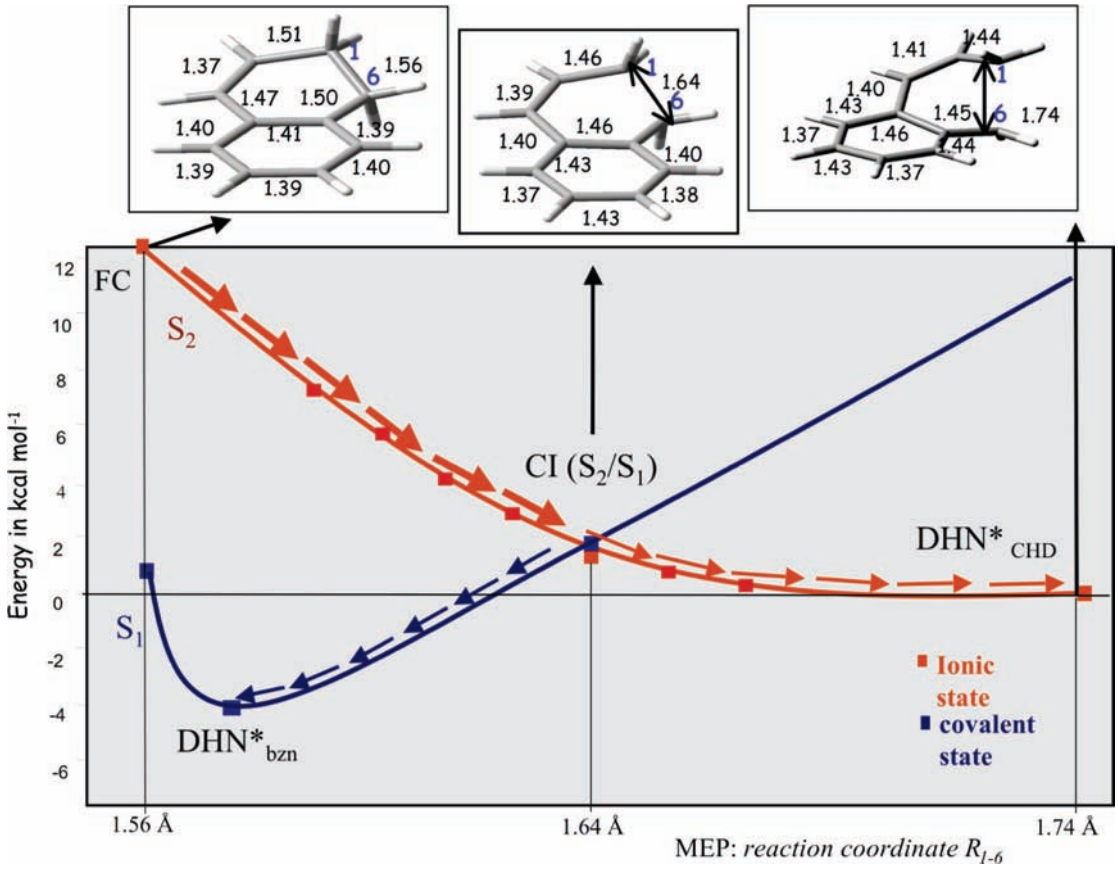


**Figure 5.** CASPT2//CASSCF energy profile for the MEP describing the relaxation path from the $S_2$ Franck−Condon (FC) point (top left), and population splitting through an $S_2/S_1$ crossing (top middle), leading to minima of benzenic ($DHN^*_{bzn}$) or cyclohexadiene ($DHN^*_{CHD}$) character (top right). The zero energy value corresponds to the relaxed $DHN^*_{CHD}$ geometry on $S_1$.

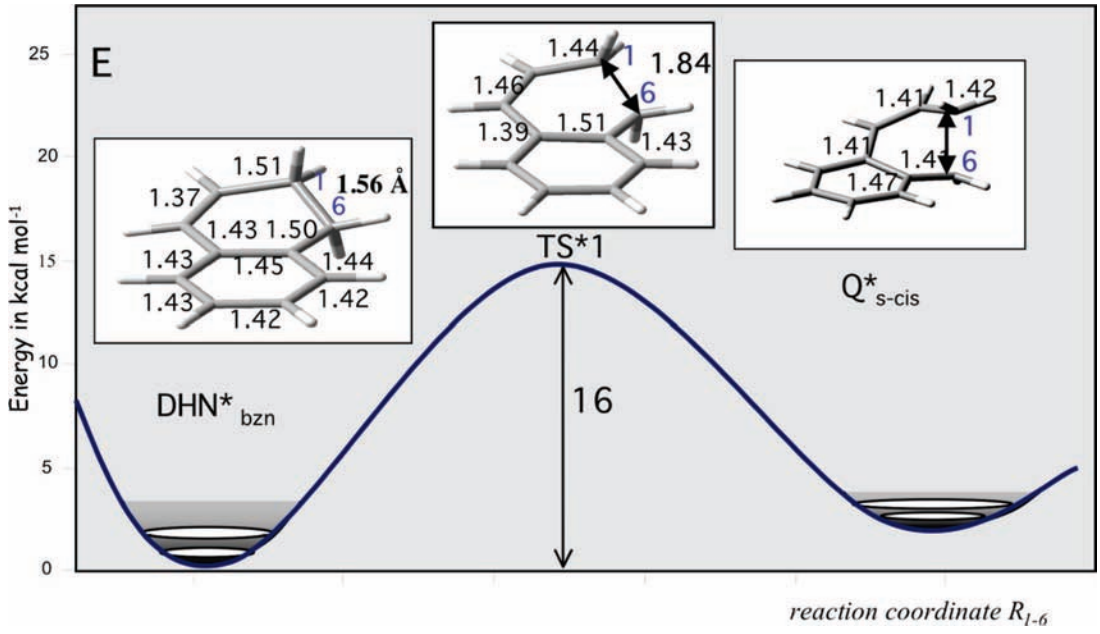


**Figure 6.** CASPT2 energy profile describing the activation barrier for the ring-opening reaction occurring adiabatically on the first excited state.

a fourth as a spectator).[52,53] The triangular kink comprises the $C_1$, $C_2$ and $C_6$ atoms for CI1 and the $C_1$, $C_5$ and $C_6$ atoms for CI2 (Figure 9). CI1 is probably lower in energy because the delocalized aromatic structure of the benzene ring is preserved. Thus, we expect this funnel identifies the most relevant radiationless decay route for DHN. Furthermore, a strong similarity exists between CI1 and the low-energy $S_1/S_0$ CI responsible for the analogous photoinduced ring-closing/ring-opening electrocyclic reaction in cZc-hexatriene/cyclohexadiene.[13]

Ground-state relaxation from the lowest energy CI[54] (CI1) may involve, in principle, three different routes as illustrated in Figure 10. Each route is associated with a specific bond formation process, which is in turn driven by a different

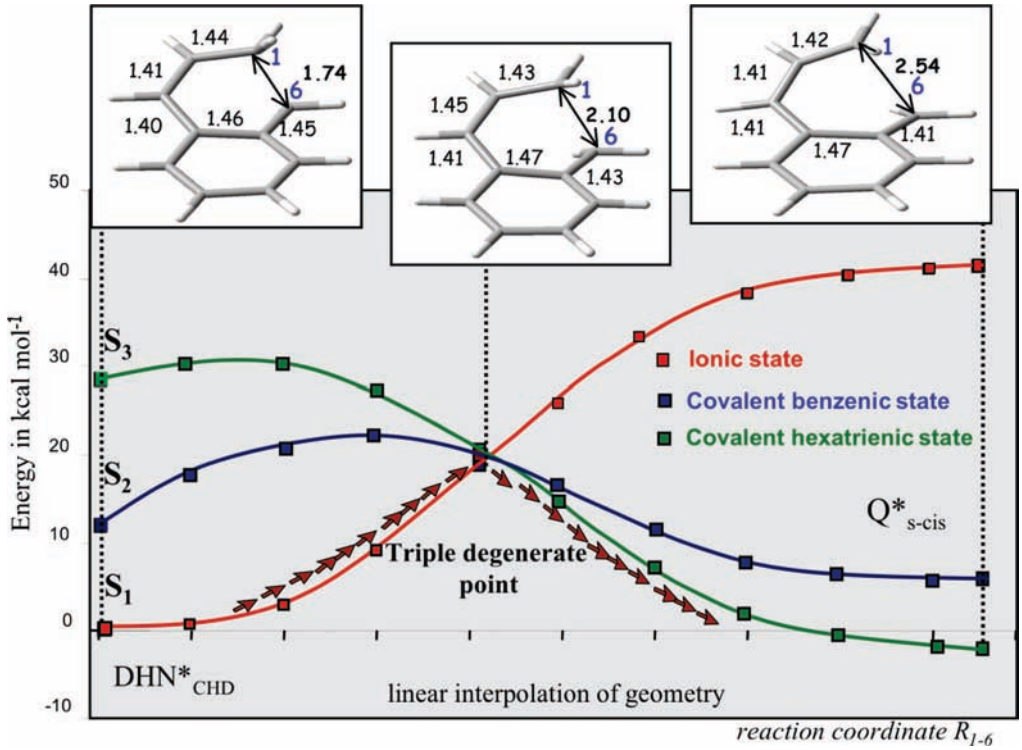


**Figure 7.** CASPT2 energy profiles calculated along a linear interpolation between the S1 minima DHN*CHD and Q*s-cis. All bond lengths are in Å.

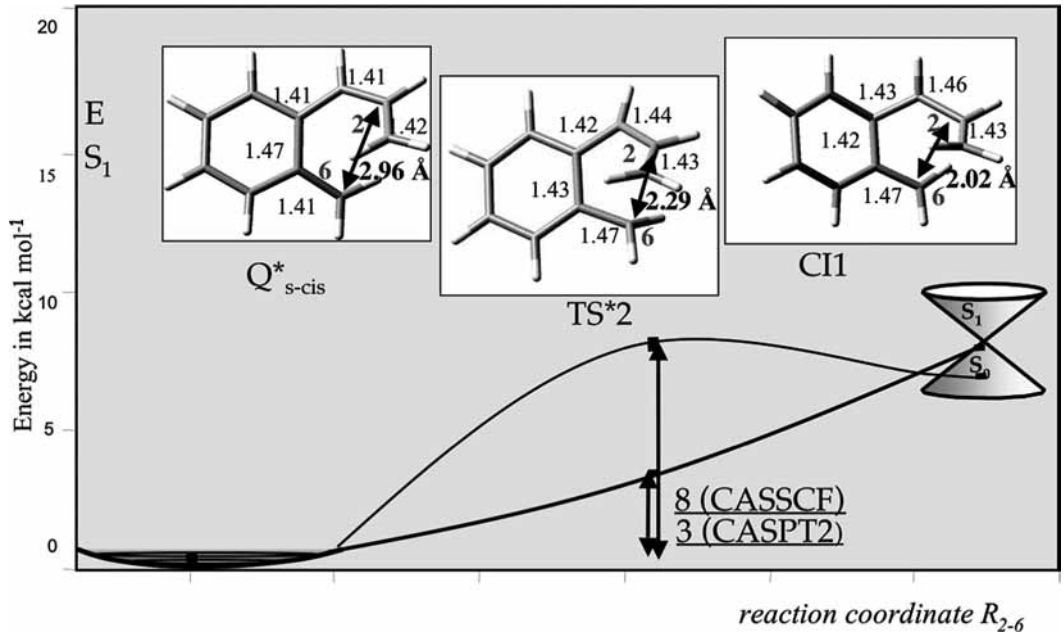


**Figure 8.** CASSCF and CASPT2 energy profiles for the reaction path connecting the $Q^*_{s\text{-}cis}$ minimum (taken as the energy zero) to CI1. The reaction coordinate is dominated by $R_{2-6}$.

recoupling pattern of the four weakly interacting electrons. Thus, it appears possible to rationalize the observed photoproducts collected on the ground state: (i) DHN back formation, (ii) the irreversible production of the tricyclic (BBH) system, and (iii) the open ring isomer (i.e., the benzoquinodimetane derivative $Q_{s\text{-}cis}$), corresponding to $C_1-C_6$, $C_2-C_6$ and $C_1-C_2$ bond formation, respectively.

Finally, we located three other $S_1/S_0$ crossings (shown in Figure S2), where the triangular "kink" is located elsewhere (see Figure S2 in the Supporting Information). One (CI3) is another cyclohexadiene-like crossing and the other two (CI4−5) involve the benzene ring and are similar to those previously found in aromatic systems.[55] These conical intersections are significantly higher in energy than CI1 (Table 2) and are likely to be unreactive. With CASPT2, CI4 is comparable in energy to the secondary CI2 identified above, although still 10 kcal/mol above CI1. During the MMVB dynamics simulations described below, none of these additional crossing regions were encountered. Thus, they do not appear to be reactive directly, so we have not considered them further.

**3.4. MMVB Dynamics.** Despite the limitations mentioned in the Computational Details, MMVB dynamics may provide a

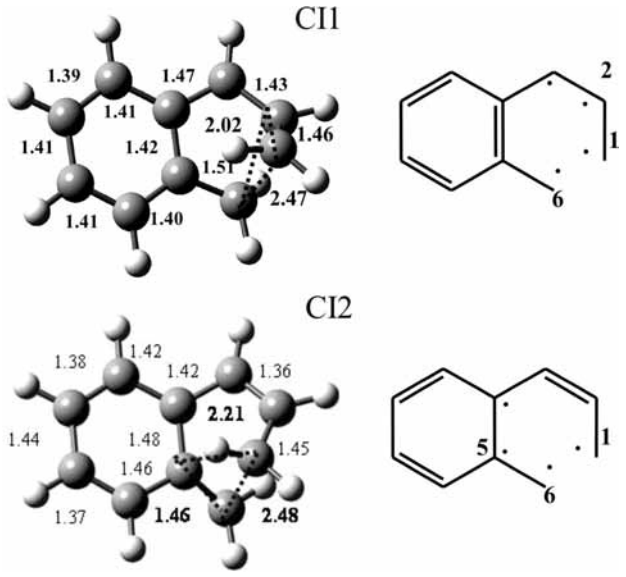


**Figure 9.** Molecular geometry and electronic structure for CI1 and CI2. The typical triangular "kinked" arrangement is shown by dotted lines.

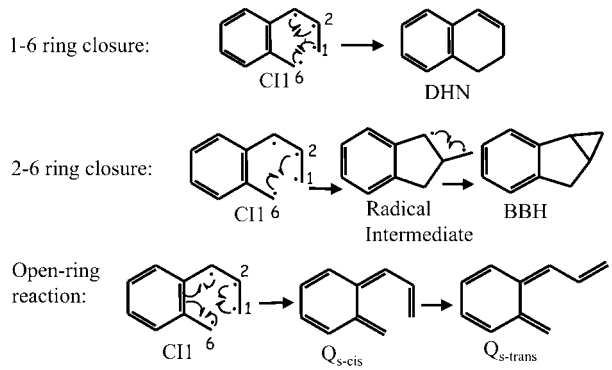


**Figure 10.** Different possible ground-state recoupling schemes from the lowest energy CI (CI1) leading to the three main photoproducts observed.

useful tool to sample the potential energy surface of the lower photochemically relevant (covalent) excited state, allowing a deeper insight into the mechanism of the nonadiabatic process, i.e., the surface hop to the ground state in the $S_1/S_0$ crossing region. Simulations were started from TS*1 and the s-cis open-ring FC region, and the results are summarized in Scheme 1 (and Table S2).

Trajectories starting from TS*1 mainly hop to $S_0$ through CI2 or CI1, within a simulation time of around 3 ps. Similar results were obtained for trajectories starting from the open-ring side (from FC/$Q_{s\text{-}cis}$). From both conical intersections, we observe the formation of both open-ring and closed-ring products, in roughly equal proportions, in agreement with the experimental quantum yields (0.2−0.6). Once the system hits the crossing seam, the photoproduct formed depends on both the velocity and the specific geometry at which the hop occurs. Analysis of all of the hop geometries (Tables S3 and S4) shows that they can be grouped into two principal sets of molecular structures, mainly differing in the $C_1-C_5$ interatomic distance. The ones with the shorter $C_1-C_5$ distance lead mainly to the closed-ring (1−5) photoproduct, whereas the ones where this distance is longer lead mainly to the open-ring and the closed-ring (1−6/2−6) isomers.

The easier accessibility of the CI2-type crossing seam as revealed by trajectory computations may be an artifact of the MMVB force field, because it swaps the order of stability of the two crossing points CI1 and CI2 with respect to the ab initio (CASSCF and CASPT2) results (Table 2). However, it is worth noting that both crossings are close in energy whatever the method used, and it is likely that they are both accessible dynamically. We have some confidence in the MMVB dynamics results, at least on a qualitative ground.[41,56]

In conclusion, dynamical MMVB results for the photoinduced ring-closing/ring-opening processes of 1,2-dihydronaphthalene show that decay to $S_0$ occurs by hitting an $S_1/S_0$ crossing seam, which extends over a wide range of nuclear configurations and is reached through a broad valley along a coordinate that is orthogonal to the initial reaction path. This dynamical behavior is illustrated in Figure 11. Thus, a typical trajectory may be described by the following steps (see also Figure S1 for some representative snapshots along a typical trajectory): (i) From TS*1 or the $Q_{s\text{-}cis}$ geometry on $S_1$, it reaches the region of the excited-state minimum ($Q^*_{s\text{-}cis}$) very quickly (within a few femtoseconds); (ii) the molecule spends most of the time there before the energy is redistributed to different modes (this is the time needed for IVR to occur); (iii) once the mode leading to TS*2 or TS*3 is populated and the corresponding energy barrier is passed, the molecule reaches the crossing region by hitting the seam at different geometries (which are of CI1 or CI2 type). The crossing seam is preserved in a $3N - 8$ dimensional subspace of the internuclear coordinates and extends over a wide range of geometries: inspection of Tables S3 and S4 shows that the hop occurs for a wide range of $C_1-C_6$ bond length (from 1.97 to 2.58 Å). Because of the range of geometries at which surface hops occur in our simulation, these crossings most likely represent different regions of the same crossing seam, although we have not tested for this further. Because the $S_1/S_0$ crossing seam is central with respect to the bond formation/breaking process, closed-ring and open-ring processes are expected to occur with similar rates and efficiency (i.e., ∼50% QY).

## 4. Conclusions

1,2-Dihydronaphthalene (DHN) was investigated by studying the photochemical $S_2 \rightarrow S_1 \rightarrow S_0$ ring-opening through reaction path computations with CASPT2//CASSCF and nonadiabatic molecular dynamics simulations with MMVB. An extended and indirectly accessible $S_1/S_0$ crossing region appears to be responsible for internal conversion to the ground state, and hence the low fluorescence quantum yields observed and products formed. Absorption of a single photon is sufficient for this.

To reach the $S_1/S_0$ crossing seam, the initial ring-opening (i.e., $C_1-C_6$ bond breaking) coordinate must be abandoned in favor of a different $C_1-C_5$ (or $C_2-C_6$) coordinate. This changeover of coordinates takes place in the region of an excited-state minimum $Q^*_{s\text{-}cis}$, the lifetime of which is related to the time taken for vibrational energy from $C_1-C_6$ to redistribute into the $C_1-C_5$ (or $C_2-C_6$) coordinates taking the system to the crossing seam.

The main results of this study are presented in Figure 12 and can be summarized as follows:

(i) The ring opening reaction begins on the spectroscopic state $S_2$: an ionic $1B_2$ hexatriene-like state absorbing at around 260 nm.

(ii) An intermediate ($DHN^*_{CHD}$) along the ring-opening path exists on this state, which is responsible for the less intense peak of the fluorescence spectrum around 400 nm.

(iii) A benzene-like unreactive (dark) excited-state $S_1$ exists in the FC region which can trap photoexcited molecules,

**SCHEME 1**

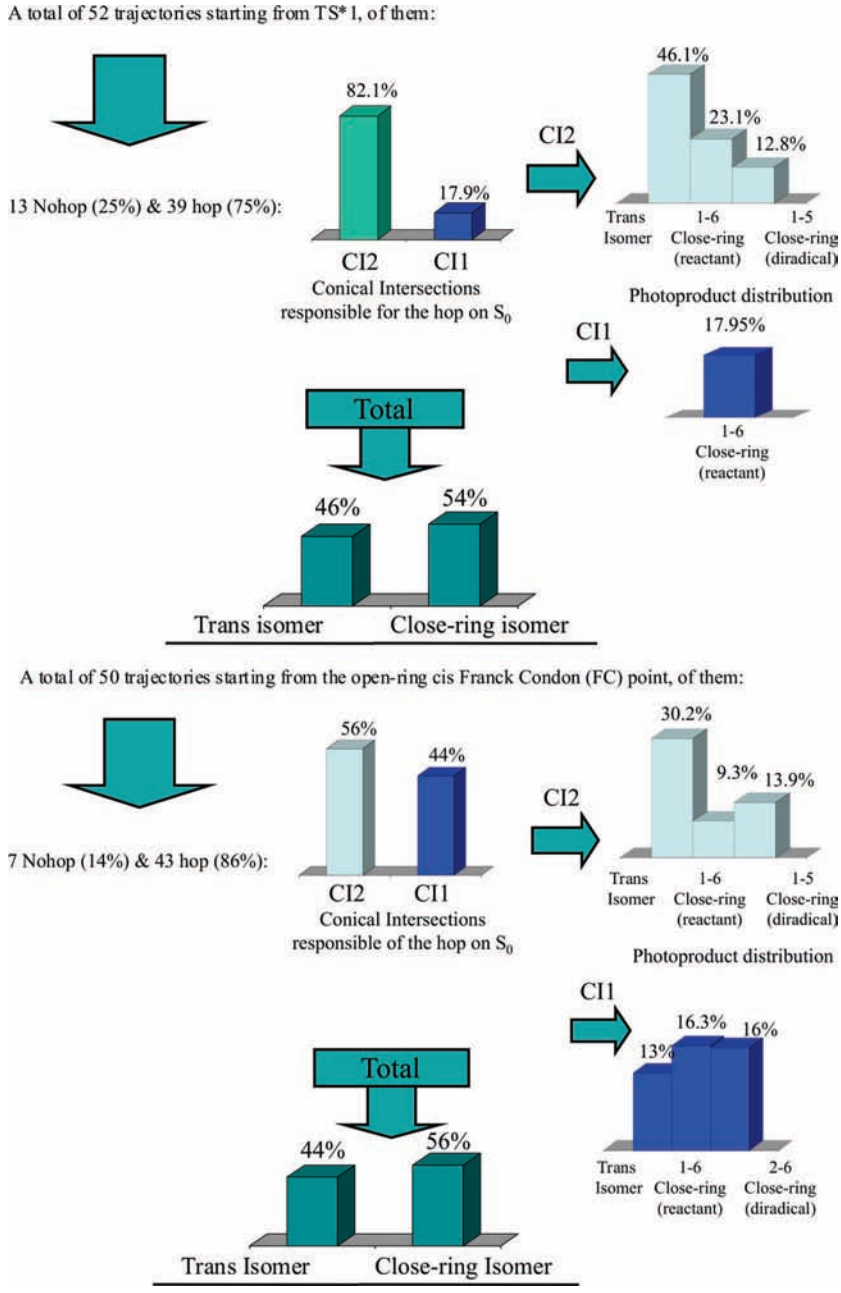


explaining the main peak of the weak fluorescence, observed around 300 nm.

(iv) The ring opening process is completed on a dark covalent ($2A_1$ hexatriene-like) excited state, where an open-ring intermediate $Q^*_{s\text{-}cis}$ exists.

(v) From $Q^*_{s\text{-}cis}$, new channels on $S_1$ are accessible which are orthogonal to the ring-opening path, leading the system into a low-energy $S_1/S_0$ real crossing region. The accessibility of the crossing explains the weakness of the observed fluorescence, whereas the shape of the crossing explains the formation of multiple products.

(vi) $S_1 \rightarrow S_0$ nonadiabatic dynamics simulations reveal that IVR on $S_1$ controls the internal conversion process and the time scale of the photochemical reaction.

(vii) Dynamic simulation of the photoproduct distribution reveals that almost the same quantum yield must be expected for the formation of both open-ring and closed-ring isomers (i.e., they have almost the same probability to be formed upon radiationless decay), whereas the bicyclic BBH isomer must be seen as a side (less probable) product. This is roughly in agreement with the experimentally observed quantum yields (0.2−0.6 for open-ring photoproduct formation).

All points i−vii above relate to the photochromic potential of DHN.[16] Because the initial relaxation direction is lost and partial vibrational equilibration has to take place in the region of a central excited-state minimum, open- and closed-ring reactants can both lead to open- and closed-ring products via internal conversion. There appears to be no strong correlation between a particular reactant and a particular product. (Here, DHN differs from the diarylethylenes we have also studied,[9] where access to the crossing is also indirect, but the crossing has a different shape). Furthermore, from the closed-ring side, the reaction path can bifurcate[57] to give a "trap" structure that fluoresces. Finally, there is an additional trap on the ground state in the formation of the 3-ring BBH. All of these factors limit the photochromic potential of DHN, as was also found

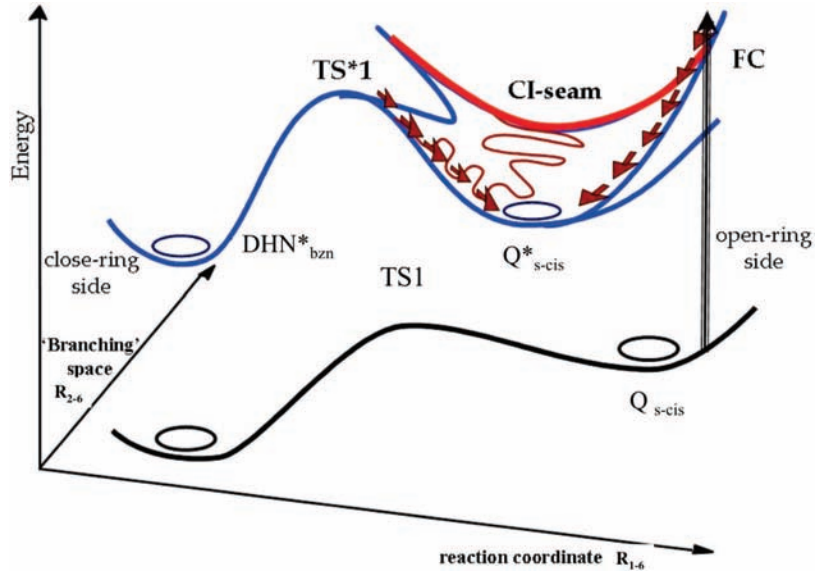


**Figure 11.** Illustration of the computed MMVB dynamics steps on the covalent excited state. The system first reaches the same minimum ($Q^*_{s\text{-}cis}$) along the $R_{1-6}$ coordinate from both sides; then IVR occurs and the system encounters the crossing seam. After the hop occurs, both closed- and open-ring products are observed.

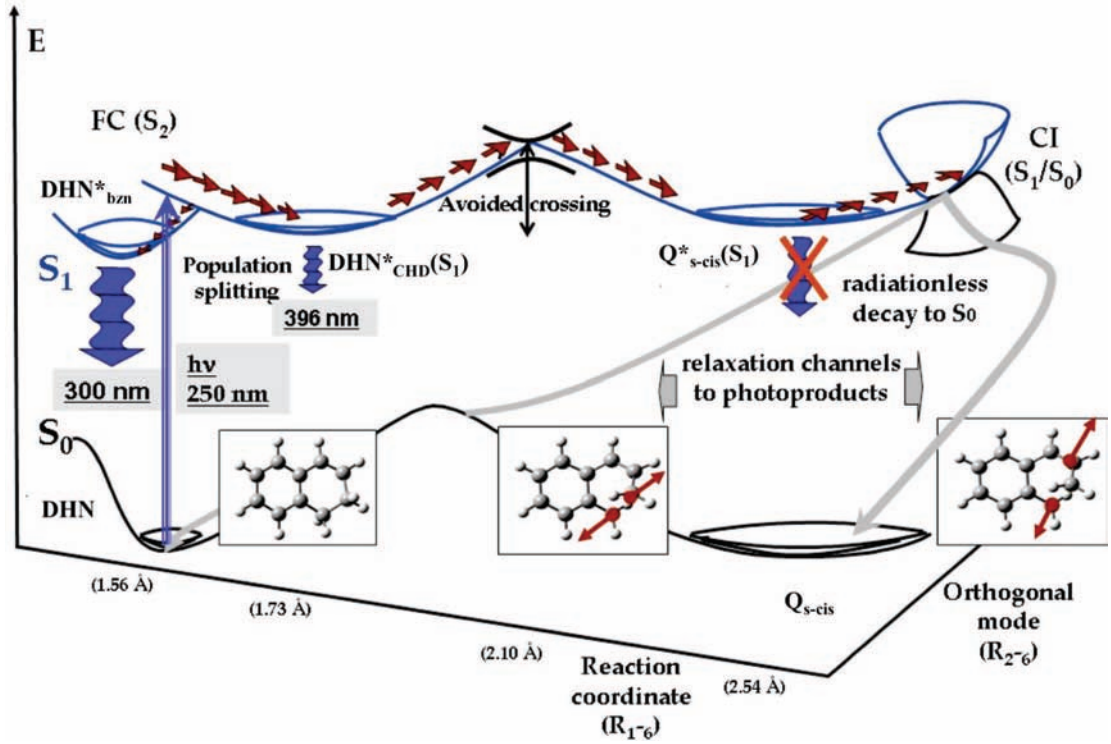


**Figure 12.** DHN photophysics and photochemistry, based on the calculations presented here.

for phenylbutadiene[25] (which was studied as a prototype photochromic fulgide).

**Acknowledgment.** The support by funds from Bologna University (Progetti Strategici d'Ateneo 2005: Progetto CompRenDe) is gratefully acknowledged. G.T.'s visit to London was supported by the EU ERASMUS program.

**Supporting Information Available:** Absolute energies of all critical structures, detailed results of trajectory calculations, and a figure showing the structures CI3, CI4 and CI5. This material is available free of charge via the Internet at http://pubs.acs.org.

## References and Notes

(1) Irie, M. *Chem. Rev.* **2000**, *100*, 1685–1716.
(2) *Photochromism, Molecules and systems*, 2nd ed. Dürr, H., Bouas-Laurent, H.,Eds.; Elsevier: Amsterdam, 2003.
(3) Bouas-Laurent, H.; Durr, H. *Pure Appl. Chem.* **2001**, *73*, 639–665.
(4) Hoffmann, R. *Angew. Chem., Int. Ed.* **2004**, *43*, 6586–6590.
(5) Woodward, R. B.; Hoffmann, R. *Angew. Chem., Int. Ed.* **1969**, *81*, 797.
(6) Yokoyama, Y. *Chem. Rev.* **2000**, *100*, 1717–1739.
(7) Heller, H. G.; Oliver, S. *J. Chem. Soc., Perkin Trans. 1* **1981**, 197–202.
(8) Heller, H. G.; Szewczyk, M. *J. Chem. Soc., Perkin Trans. 1* **1974**, 1487–1492.
(9) Boggio-Pasqua, M.; Ravaglia, M.; Bearpark, M. J.; Garavelli, M.; Robb, M. A. *J. Phys. Chem. A* **2003**, *107*, 11139–11152.

(10) Ern, J.; Petermann, M.; Mrozek, T.; Daub, J.; Kuldova, K.; Kryschi, C. *Chem. Phys.* **2000**, *259*, 331–337.

(11) Boggio-Pasqua, M.; Bearpark, M. J.; Hunt, P. A.; Robb, M. A. *J. Am. Chem. Soc.* **2002**, *124*, 1456–1470.

(12) De Waele, V.; Schmidhammer, U.; Mrozek, T.; Daub, J.; Eberhard, R. T. *J. Am. Chem. Soc.* **2002**, *124*, 2438–2439.

(13) Garavelli, M.; Celani, P.; Fato, M.; Bearpark, M. J.; Smith, B. R.; Olivucci, M.; Robb, M. A. *J. Phys. Chem. A* **1997**, *101*, 2023–2032.

(14) De Waele, V.; Beutter, M.; Schmidhammer, U.; Riedle, E.; Daub, J. *Chem. Phys. Lett.* **2004**, *390*, 328–334.

(15) Daub, J.; Knochel, T.; Mannschreck, A. *Angew. Chem., Int. Ed. Engl.* **1984**, *23*, 960–961.

(16) Gorner, H.; Mrozek, T.; Daub, J. *Chem.—Eur. J.* **2002**, *8*, 4008–4016.

(17) Kleinhuis, H.; Wijting, R. L. C.; Havinga, E. *Tetrahedron Lett.* **1971**, 255.

(18) Duguid, R. J.; Morrison, H. *J. Am. Chem. Soc.* **1991**, *113*, 1271–1281.

(19) Salisbury, K. *Tetrahedron Lett.* **1971**, 737.

(20) Tinland, B.; Decoret, C. *Tetrahedron Lett.* **1971**, 3019.

(21) Seeley, D. A. *J. Am. Chem. Soc.* **1972**, *94*, 4378.

(22) Laarhoven, W. H.; Berendsen, N. *Recl. Trav. Chim. Pays-Bas* **1986**, *105*, 367–371.

(23) Duguid, R. J.; Morrison, H. *J. Am. Chem. Soc.* **1991**, *113*, 1265–1271.

(24) Robb, M. A.; Bearpark, M. J.; Celani, P.; Bernardi, F.; Olivucci, M. *Mol. Cryst. Liq. Cryst.* **2000**, *344*, 31–39.

(25) Ogliaro, F.; Wilsey, S.; Bearpark, M. J.; Sardo-Infirri, S. *Mol. Phys.* **2006**, *104*, 1017–1032.

(26) Boggio-Pasqua, M.; Bearpark, M. J.; Robb, M. A. *J. Org. Chem.* **2007**, *72*, 4497–4503.

(27) Celani, P.; Robb, M. A.; Garavelli, M.; Bernardi, F.; Olivucci, M. *Chem. Phys. Lett.* **1995**, *243*, 1–8.

(28) Frisch, M. J; Trucks, G. W.; Schlegel, H. B.; Scuseria, G. E.; Robb, M. A.; Cheeseman, J. R.; Montgomery, J. A., Jr.; Vreven, T.; Kudin, K. N., Burant, J. C.; Millam, J. M.; Iyengar, S. S.; Tomasi, J.; Barone, V.; Mennucci, B.; Cossi, M.; Scalmani, G.; Rega, N.; Petersson, G. A.; Nakatsuji, H.; Hada, M.; Ehara, M.; Toyota, K.; Fukuda, R.; Hasegawa, J.; Ishida, M.; Nakajima, T.; Honda, Y., Kitao, O.; Nakai, H.; Klene, M.; Li, X.; Knox, J. E.; Hratchian, H. P.; Cross, J. B.; Bakken, V.; Adamo, C.; Jaramillo, J.; Gomperts, R.; Stratmann, R. E.; Yazyev, O., Austin, A. J., Cammi, R., Pomelli, C., Ochterski, J. W., Ayala, P. Y., Morokuma, K., Voth, G. A., Salvador, P., Dannenberg, J. J., Zakrzewski, V. G., Dapprich, S., Daniels, A. D., Strain, M. C., Farkas, O., Malick, D. K., Rabuck, A. D., Raghavachari, K., Foresman, J. B., Ortiz, J. V., Cui, Q., Baboul, A. G., Clifford, S., Cioslowski, J., Stefanov, B. B., Liu, G., Liashenko, A., Piskorz, P., Komaromi, I., Martin, R. L., Fox, D. J., Keith, T., Al-Laham, M. A., Peng, C. Y., Nanayakkara, A., Challacombe, M., Gill, P. M. W., Johnson, B., Chen, W., Wong, M. W., Gonzalez, C., Pople, J. A., *Gaussian 03*, Revision C.02; Gaussian Inc.,: Wallingford, CT, 2004.

(29) Andersson, K.; Barysz, M.; Bernhardsson, A.; Blomberg, M. R. A.; Cooper, D. L.; Fleig, T., Fülscher, M. P.; de Graaf, C.; Hess, B. A., Karlström, G.; Lindh, R.; Malmqvist, P.-Å., Neogrády, P.; Olsen, J.; Roos, B. O.; Sadlej, A. J., Schütz, M.; Schimmelpfennig, B.; Seijo, L., Serrano-Andrés, L.; Siegbahn, P. E. M., Stålring, J.; Thorsteinsson, T.; Veryazov, V.; Widmark, P.-O. *Molcas*, 5.0; Lund University: Sweden, 2000.

(30) Malmqvist, P. A.; Roos, B. O.; Schimmelpfennig, B. *Chem. Phys. Lett.* **2002**, *357*, 230–240.

(31) Stephens, P. J.; Devlin, F. J.; Chabalowski, C. F.; Frisch, M. J. *J. Phys. Chem.* **1994**, *98*, 11623–11627.

(32) Becke, A. D. *J. Chem. Phys.* **1993**, *98*, 5648–5652.

(33) Lee, C. T.; Yang, W. T.; Parr, R. G. *Phys. Rev. B* **1988**, *37*, 785–789.

(34) Vosko, S. H.; Wilk, L.; Nusair, M. *Can. J. Phys* **1980**, *58*, 1200–1211.

(35) Levine, B. G.; Ko, C.; Quenneville, J.; Martinez, T. J. *Mol. Phys.* **2006**, *104*, 1039–1051.

(36) Dreuw, A.; Head-Gordon, M. *Chem. Rev.* **2005**, *105*, 4009–4037.

(37) Boggio-Pasqua, M.; Bearpark, M. J.; Ogliaro, F.; Robb, M. A. *J. Am. Chem. Soc.* **2006**, *128*, 10533–10540.

(38) Hunt, P. A.; Robb, M. A. *J. Am. Chem. Soc.* **2005**, *127*, 5720–5726.

(39) Bernardi, F.; Olivucci, M.; Robb, M. A. *J. Am. Chem. Soc.* **1992**, *114*, 1606–1616.

(40) Bearpark, M. J.; Boggio-Pasqua, M. *Theor. Chem. Acc.* **2003**, *110*, 105–114.

(41) Garavelli, M.; Ruggeri, F.; Ogliaro, F.; Bearpark, M. J.; Bernardi, F.; Olivucci, M.; Robb, M. A. *J. Comput. Chem.* **2003**, *24*, 1357–1363.

(42) Bearpark, M. J.; Boggio-Pasqua, M.; Robb, M. A.; Ogliaro, F. *Theor. Chem. Acc.* **2006**, *116*, 670–682.

(43) Bearpark, M. J.; Ogliaro, F.; Vreven, T.; Boggio-Pasqua, M.; Frisch, M. J.; Larkin, S. M.; Morrison, M.; Robb, M. A. *J. Photochem. Photobiol. A: Chem.* **2007**, *190*, 207–227.

(44) Tully, J. C.; Preston, R. K *J. Chem. Phys.* **1971**, *55*, 562.

(45) Tully, J. C. *Faraday Discuss.* **2004**, *127*, 463–466.

(46) Bearpark, M. J.; Robb, M. A.; Bernardi, F.; Olivucci, M. *Chem. Phys. Lett.* **1994**, *217*, 513–519.

(47) Deumal, M.; Bearpark, M. J.; Smith, B. R.; Olivucci, M.; Bernardi, F.; Robb, M. A. *J. Org. Chem.* **1998**, *63*, 4594–4600.

(48) Helgaker, T.; Uggerud, E.; Jensen, H. J. A. *Chem. Phys. Lett.* **1990**, *173*, 145–150.

(49) Preston, R. K.; Tully, J. C. *J. Chem. Phys.* **1971**, *54*, 4297.

(50) Celani, P.; Bernardi, F.; Robb, M. A.; Olivucci, M. *J. Phys. Chem.* **1996**, *100*, 19364–19366.

(51) Bearpark, M. J.; Bernardi, F.; Clifford, S.; Olivucci, M.; Robb, M. A.; Smith, B. R.; Vreven, T. *J. Am. Chem. Soc.* **1996**, *118*, 169–175.

(52) Garavelli, M.; Bernardi, F.; Cembran, A.; Castano, O.; Frutos, L. M.; Merchan, M.; Olivucci, M. *J. Am. Chem. Soc.* **2002**, *124*, 13770–13789.

(53) Bearpark, M. J.; Bernardi, F.; Clifford, S.; Olivucci, M.; Robb, M. A.; Vreven, T. *J. Phys. Chem. A* **1997**, *101*, 3841–3847.

(54) Ruiz, D. S.; Cembran, A.; Garavelli, M.; Olivucci, M.; Fuss, W. *Photochem. Photobiol.* **2002**, *76*, 622–633.

(55) Palmer, I. J.; Ragazos, I. N.; Bernardi, F.; Olivucci, M.; Robb, M. A. *J. Am. Chem. Soc.* **1993**, *115*, 673–682.

(56) Garavelli, M.; Bernardi, F.; Olivucci, M.; Bearpark, M. J.; Klein, S.; Robb, M. A. *J. Phys. Chem. A* **2001**, *105*, 11496–11504.

(57) Migani, A.; Bearpark, M. J.; Olivucci, M.; Robb, M. A. *J. Am. Chem. Soc.* **2007**, *129*, 3703–3713.

JP802613M